CHEMISTRY OF MATERIALS

pubs.acs.org/cm

Article

Polycarbosilane-Grafted Nanoparticles: Free-Flowing Hairy Nanoparticle Liquids That Convert to Ceramic

Kara L. Martin, Dayton P. Street, and Matthew B. Dickerson*

Cite This: *Chem. Mater.* 2020, 32, 3990–4001

Read Online

ACCESS | Metrics & More | Article Recommendations | Supporting Information

ABSTRACT: Here, we report a new class of hybrid nanoparticles (NPs) that are self-supporting and display viscous flow behavior in the absence of solvent, yet convert to a purely inorganic material on heating. Hairy nanoparticles (HNPs) composed of silica nanoparticle cores (10–20 nm diameter) and preceramic poly(1,1-dimethylpropylsilane) (l-PCS) brushes were synthesized via a grafting-from approach utilizing hydrosilylation chemistry. The l-PCS polymer brush was grown from the nanoparticle core by anchoring the Pt(0) Karstedt's catalyst to Si–H groups functionalized on the silica surface. The resulting l-PCS-based HNPs were easily dispersed in a variety of organic solvents, displaying Newtonian rheological behavior at low weight percent solvent loadings, while neat HNPs displayed relatively low viscosities. The Krieger–Dougherty equation was used to evaluate viscosity trends as related to corona size, with the corona size being determined through dynamic light scattering. Thermally cured HNPs were successfully converted to SiO_2/SiC nanocomposites, as evidenced by X-ray diffraction and attenuated total reflection (ATR)-Fourier transform infrared (FTIR). These unique preceramic HNPs hold considerable promise as a route to high-temperature materials, offering enhanced processability and compositional tailorability compared to neat resins.

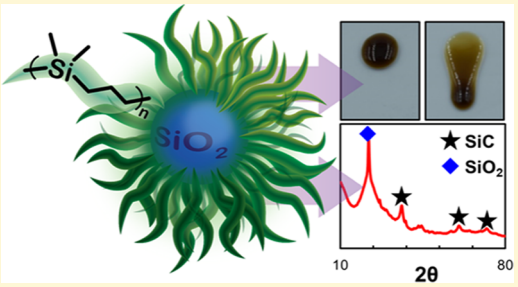

INTRODUCTION

For nearly 50 years, preceramic polymers have been developed and used for fabricating high-performance, nonoxide ceramics in both academic and industrial settings.[1] Preceramic polymers have proven to be advantageous for ceramic formulation over the more common powder methods due to ease of processing, tailorable chemistry, and microstructural control.[2−9] Indeed, these macromolecules provide a diverse array of structures rich in atoms such as Si, C, O, B, and N that can yield metastable, solid-state compositions that are impossible to obtain via powder processing (e.g., SiNC).[10−13] A variety of straightforward and robust synthetic pathways have been defined for preparing preceramic polymers, including Pt(0)-catalyzed hydrosilylations,[14,15] Grignard couplings,[16] and anionic or Pt(0)-catalyzed ring-opening polymerizations.[17−19] Synthetic design of the polymer side chains and overall backbone structure (linear, hyperbranched, block-copolymer) aids in the control of the rheological, thermal, and processing properties of the polymer.[2,5,20,21] Additionally, the incorporation of cross-linkable moieties into the preceramic molecular architecture is important as the effective curing of these precursors has been noted to increase mass yields in the polymer-to-ceramic conversion process.[2,5,20,21] Preceramic polymers can be processed with common polymer fabrication methods, including coating, additive manufacturing, and infiltration.[22−25] Subsequent to forming methods, the preceramic polymer is cured at ∼100–400 °C and then pyrolyzed at temperatures >600 °C.[26] Additional heat treatments >1000 °C can be utilized to crystallize the polymer-derived ceramic and yield materials with composition and properties determined by the initial preceramic polymer.[26]

Though they present many advantages, including the spinning of advanced SiC fibers,[27,28] preceramic polymers are not without drawbacks. For example, the thermal conversion of the polymer to a ceramic typically results in significant weight loss and volume shrinkage due to the gaseous release of organic components of the polymer. This release of organic gases such as ethane, methane, and carbon monoxide from the bulk piece leads to porosity that can make materials susceptible to cracking.[29] Densification of the polymer chains through chemical cross-linking is one method of improving the ceramic yield and limiting volume shrinkage by reducing organic volatilization from the polymer chains.[30,31] The shrinking and cracking of the preceramic polymer as it converts to inorganic have important consequences in the fabrication of ceramic composites. Preceramic polymers are utilized to form the matrix of ceramic composites through a processing method known as polymer infiltration and pyrolysis (PIP). The PIP

Received: February 7, 2020
Revised: April 8, 2020
Published: April 9, 2020

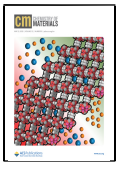

https://dx.doi.org/10.1021/acs.chemmater.0c00528
Chem. Mater. 2020, 32, 3990–4001

process involves flowing low-viscosity preceramic polymer into porous ceramic pieces (e.g., laid-up fiber preforms), where it is cured and pyrolyzed to yield ceramic. The shrinking of the preceramic polymer requires many cycles of infiltration (up to 10) to reduce the porosity of the original piece and yield dense parts.[32] As each PIP cycle consumes raw materials and requires labor, preceramic polymer deficiencies can increase the cost of composite manufacture considerably.

One method to mitigate shrinkage and cracking associated with the conversion of polymers to ceramics is to physically mix ceramic powders into the preceramic polymer before pyrolysis (i.e., this reduces the amount of polymer and thus the amount of shrinkage). Including ceramic powders that are chemically distinct from the preceramic polymer also aids in diversifying the final ceramic composite and can improve properties such as flexural strength and toughness.[33−35] Further, the use of reactive powders or "active fillers" that adsorb and react with the organic gases released during pyrolysis can also be used to offset preceramic polymer shrinkage.[36,37] However, ceramic powders are typically hydrophilic and therefore may suffer chemically compatibility issues with hydrophobic preceramic polymers. The poor entropy of mixing between ceramic powders and preceramic polymers results in these powder−polymer slurries having significantly higher viscosities and more solid-like characteristics than the neat resins. Such rheological behavior represents a significant deviation from the Newtonian behavior exhibited by most neat macromolecular ceramic precursors.[38−40] The increased viscosity is due to particle flocculation within the composite, which disrupts the flow field of the neat polymer.[41] Composites processed from poorly dispersed powders/preceramic polymer slurries can yield inhomogeneous and irreproducible microstructures.[42] In one example, a ZrB_2−polycarbosilane slurry with poorly dispersed particles was used to fabricate carbon fiber/ceramic composites.[43] The resulting ceramic had carbon fiber coated with either SiC from the carbosilane or ZrB_2. This resulted in two distinct phases with the more SiC-rich interface oxidizing readily to SiO_2, which thereby reduced the resistance of the composite to erosion and oxidation, relative to fiber tows infiltrated with ZrB_2 uniformly dispersed in water.

A method to improve the chemical compatibility of inorganic nano- or microparticles with the surrounding polymer or organic solvent matrix is the chemical modification of particle surfaces with polymers or ligands.[44] Attaching polymers or ligands to a particle surface can be accomplished by several different grafting polymerizations (e.g., grafting-to, grafting-from, or grafting-through methods).[45] Grafting chemistries are diverse and can accommodate a wide variety of systems and conditions, making this technique an effective and accessible method for coating particle surfaces. Grafting methods are well developed for a variety of canonical polymers (e.g., polystyrene and poly(methyl methacrylate)) on a range of inorganic and organic nano- and microparticles.[46−51] Additionally, it is well understood how grafting density, polymer chain length, and particle morphology affect the overall rheological, dispersion, and mechanical properties of the grafted systems.[52,53] In the following work, graft-from polymerization was selected due to the ability to achieve the high grafting densities necessary to effectively disperse functionalized nanoparticles (NPs).

Grafting to improve particle stability in preceramic polymer matrices is an underdeveloped field. There are a range of papers detailing the grafting of poly(dimethylsiloxane) to particles for applications in high-performance elastomers, but conversion to ceramics is not explored.[54,55] To our knowledge, only five papers exist describing the grafting of preceramic polycarbosilanes to particle surfaces,[18,19,56−58] with only two reporting conversion of the particles to ceramics.[19,56] Additionally, polycarbosilane grafting typically takes place on microparticles, with the smallest particles studied being 20−40 nm gold particles.[57] Establishing robust grafting routes for formulating dispersible preceramic-grafted particles and expanding on the characterization of such materials will elucidate novel ceramic materials with tailorable compositions and enhanced processing characteristics.

This report details the synthesis of poly(1,1-dimethylpropylsilane) (l-PCS)-grafted hairy nanoparticles (HNPs), the characterization of these particles, and their conversion to SiC/SiO_2 composites. Silica nanoparticles with diameters of ∼10−20 nm were used, and the polymer corona was covalently grown from the surface of the silica nanoparticles through hydrosilylation chemistry. Attenuated total reflection (ATR)-Fourier transform infrared (FTIR), ^{1}H NMR, dynamic light scattering (DLS), viscosity profiling, thermal gravimetric analysis (TGA), differential scanning calorimetry (DSC), and electron microscopy were used to characterize the HNPs, as well as highlight the favorable dispersibility and rheological properties of this new class of preceramic HNPs. X-ray diffraction (XRD) was used to show the successful conversion of the l-PCS corona to SiC upon pyrolysis. The facile chemistry reported here represents a straightforward pathway to free-flowing preceramic polymer-based hybrid liquids featuring relatively high loadings of inorganic nanoparticles that can be heat-treated to yield inorganic composites.

EXPERIMENTAL SECTION

Chemicals and Reagents. Silica nanoparticles (10−20 nm in diameter, particles were not perfectly spherical) dispersed in toluene at 45 wt % were received from Nissan Chemical. Allyldimethylsilane was received from Gelest, Inc. and used without purification. Karstedt's catalyst, septa-sealed dichloromethylsilane, and septa-sealed toluene were received from Sigma-Aldrich and used without purification.

Functionalization of Silica Nanoparticles. Silica nanoparticles (Nissan Chemical) were stored and used in an argon glovebox to prevent the absorption of water. The silica was functionalized with silane moieties through the reaction of a small molecule silane, dichloromethylsilane, with the Si−OH functionalities on the silica surface. The silica was initially kept dry so that adventitious water did not react with the dichloromethylsilane before it could react with the silica surface. A weight ratio of 1:0.25 grams of silica to grams of dichloromethylsilane was used in this reaction. Silica dispersed in toluene was added to a round-bottom flask with an oval stir bar and rubber septa in the glovebox. The flask was placed in an oil bath at 70 °C outside of the glovebox with a nitrogen inlet. Dichloromethylsilane was added dropwise to the silica suspension while stirring. As the reaction proceeded, the solution turned light yellow with substantial bubbling. The reaction was stirred overnight. Centrifuging the silica out of toluene caused significant aggregation, making the particles difficult to redisperse in toluene. To circumvent this irreversible aggregation, the silanized silica was left in toluene and distilled under vacuum at 50 °C for 1 h to remove any unreacted small molecular silane, while leaving behind toluene. The silica, still dispersed in toluene, was then poured into a flask containing dry sodium bicarbonate and agitated by hand (washed over the Na_2CO_3) to neutralize the HCl produced as a byproduct of the silanization reaction. The action of washing the dispersion over sodium bicarbonate is reminiscent of washing an organic fraction over

https://dx.doi.org/10.1021/acs.chemmater.0c00528
Chem. Mater. 2020, 32, 3990−4001

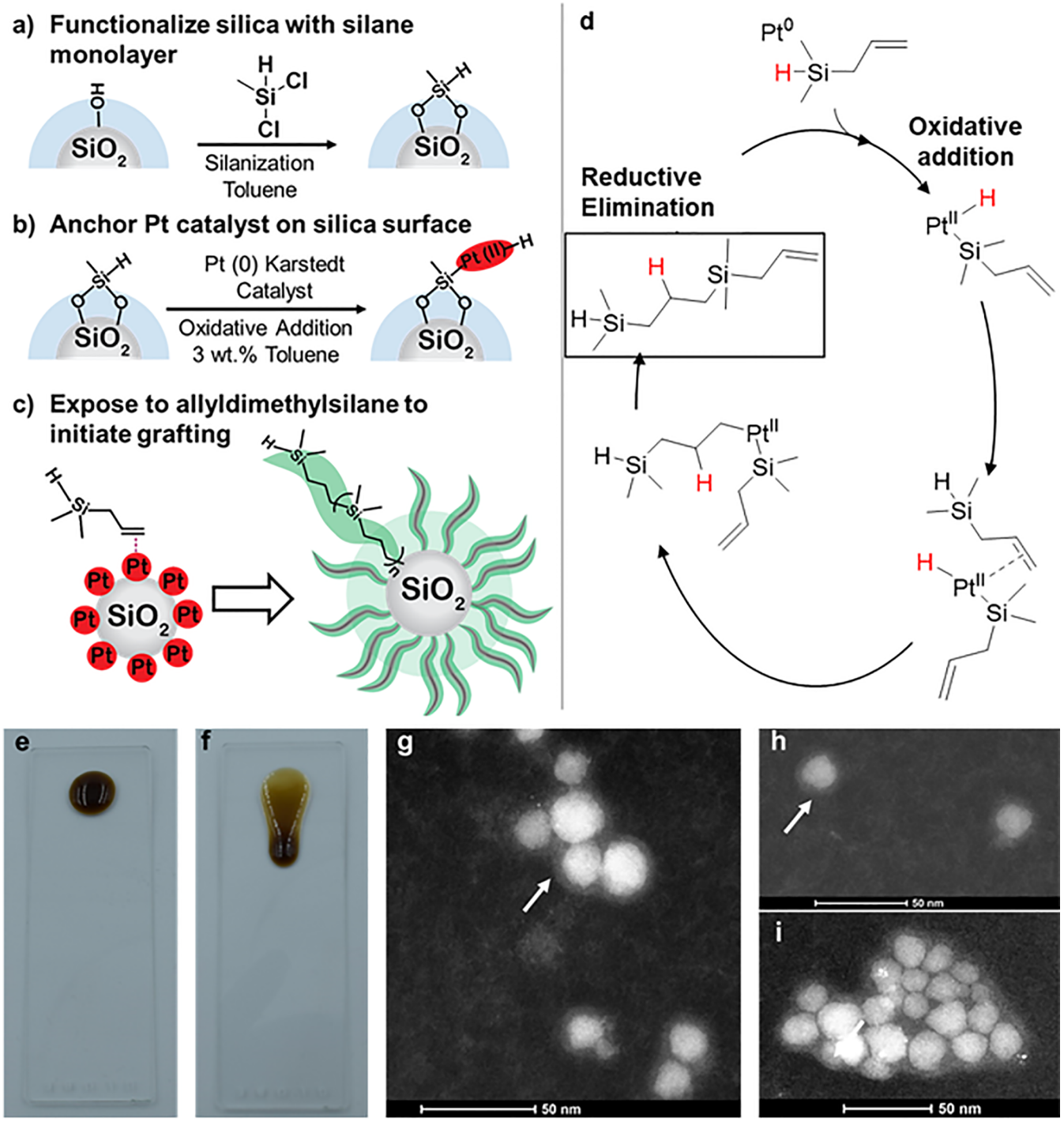

Figure 1. Illustration (left) of the silica functionalization (a), metal catalyst anchoring (b), and the growing of the preceramic l-PCS brush from the silica surface (c) alongside a schematic of the Pt(0)-catalyzed hydrosilylation mechanism (d). Neat 72-HNP dropped on a glass slide (e) and after tilting the glass slide perpendicular to the floor (f). Scanning TEM (STEM) imaging of the 72-HNP (g, h) and 48-HNP (i) show dense corona surrounding the silica nanoparticles. Single particle images (g) show corona completely surrounding the particle.

magnesium sulfate to remove water. The dispersion was washed over sodium bicarbonate several times and tested with pH paper to monitor neutralization. The final product looked similar to the original opalescent silica/toluene dispersion with a very slight yellow color.

Hydrosilylation Grafting Reaction. The weight ratios by a gram of reactants used in this grafting technique were 1:0.55:3 silica to Pt(0) to allyldimethylsilane. Silane-functionalized silica (SiH-silica) dispersed in toluene was diluted to 3 wt % with (additional) toluene in a round-bottom flask equipped with a stir bar and rubber septum. This dispersion was degassed with argon for 20 min. The dispersion was stirred at 70 °C under nitrogen or argon, and the Pt(0) Karstedt's catalyst was added dropwise. The Pt(0) catalyst was allowed to anchor into the silane moieties on the silica surface through oxidative addition over the course of 5−10 min. This changed the color of the solution from translucent to a slight yellow color, due to the oxidation of the catalyst. Leaving the catalyst to anchor for too long resulted in gelling of the reaction medium. Allyldimethylsilane was then added dropwise to the reaction flask at 70 °C, and the polymerization proceeded for 24−72 h. As the polymerization proceeded, the

https://dx.doi.org/10.1021/acs.chemmater.0c00528
Chem. Mater. 2020, 32, 3990−4001

reaction medium changed color from light yellow to dark brown. This color change happened slowly over the course of several hours. The toluene was then evaporated with rotary evaporation, and the HNPs were collected and used without further purification. The HNPs can solidify if stored improperly (e.g., HNP gel in ~24 h if left at room temperature in the neat state). Storing HNPs dispersed in toluene or dichloromethane (DCM) prevents nanoparticle gelling. HF was used to cleave the grafted polymer chains from the silica surface, but the study was inconclusive. HF treatment appeared to react with the polymer, and the "cleaved" material was undetectable by gel permeation chromatography (GPC). ^{1}H NMR 400 MHz ($CDCl_3$/toluene-d_8) −0.1 to 0.08 (Si−CH_3), 0.52 (Si−$CH_2$$CH_2$$CH_2$−Si), 1.3 (Si−$CH_2$$CH_2$$CH_2$−Si).

HNP/SMP-877 Composite Formulation. HNPs and commercial preceramic polymer SMP-877 (Starfire Systems Inc.) were weighed into a round-bottom flask equipped with a stir bar at different weight percents. HNP of 75 wt % and SMP-877 of 25 wt % were chosen for one composite and 25 wt % HNP and 75 wt % SMP-877 were used for the other sample. These samples were made on a 1 g scale. Ten milliliters of toluene was added to the mixtures, and they were thoroughly stirred for 30 min. The toluene was removed to yield a viscoelastic material. The samples were cross-linked at 160 °C for 1 h and then at 250 °C for another hour under vacuum. The cross-linked HNP/SMP-877 materials are rubbery solids.

Material Characterization. The HNP-grafted brushes before and after pyrolysis were characterized using a Bruker-Alpha P ATR-FTIR with OPUS software. Dispersed HNPs and l-PCS were characterized on a Bruker 400 MHz ^{1}H NMR. A Zetasizer Malvern Nano ZS series was used to determine the radius of hydration of the HNPs through dynamic light scattering (DLS) using a 100VA He−Ne laser with a 633 nm wavelength and a scattering angle of 175°.[59] A TA Discovery HR-3 hybrid rheometer outfitted with a cone-and-plate fixture (2° cone with a 40 mm diameter on a temperature-controlled Peltier Plate) was used to measure the viscosity profiles of several low-viscosity HNP samples dispersed in 2-ethylhexanol at 21 °C. The viscosity profiles of neat HNP samples and concentrated HNP samples dispersed in 2-ethylhexanol were determined using a parallel plate fixture with a 200 μm gap. The samples were visualized using a Talos (FEI, Portland, OR) transmission electron microscopy (TEM) operating at 200 kV on lacy carbon ultrathin grids. The samples were dispersed in tetrahydrofuran (THF) or DCM at concentrations of around 8×10^{-4} mg/mL and drop-cast onto the grid. The grid was held above a Kim Wipe to wick away the solvent and keep the particles from aggregating. The HNPs were pyrolyzed under argon in a graphite furnace at 1400 °C for 1 h after a 10 °C ramp from room temperature. X-ray diffraction patterns of the pyrolyzed HNPs were acquired on a tabletop Bruker D2 Phaser equipped with a Cu X-ray tube with a maximum of 30 kV, 10 mA. Data was collected using a 0.02 step scan from 10 to 80° with an exposure time of 1 s/step. Ceramic yield was determined for cured HNPs heated to 1000 °C on a TA Instruments Q600 thermogravimetric analysis (TGA). Samples were heated in platinum pans for 20 °C/min under an argon atmosphere (100 mL/min). DSC was completed on a TA DSC 2500 using aluminum pans, and displayed DSC traces were obtained on the second heating curve of a heat−cool−heat cycle at 10 °C from −80 to 80 °C.

RESULTS AND DISCUSSION

Synthesis of Preceramic HNPs through Hydrosilylation Chemistry. HNP synthesis was conducted via a grafting-from approach, utilizing hydrosilylation chemistry to grow poly(1,1-dimethylpropylsilane) (l-PCS) from the surface of silica nanoparticles (Figure 1a−d). These silica nanoparticle cores were initially functionalized with dichloromethylsilane via reaction with native surface hydroxyl groups to coat the silica surfaces with Si−H bonds. Functionalization was monitored through ATR-FTIR, which shows the appearance of the Si−H absorption at ~900 cm^{-1}, as well as absorptions at ~2800−3000 cm^{-1} corresponding to the methyl group included in the silane monolayer (Figure S1). TGA shows a weight loss of ~6% from 200 to 1000 °C, with an initial weight loss of ~1−2% from 0 to 200 °C corresponding to the adsorbed water (Figure S2). This mass loss corresponds to a grafting density of 16 Si−H initiation sites/nm^2. Grafting density calculations can be found in the Supporting Information (SI).[59]

After successful functionalization, a graft-from approach utilizing the Pt-catalyzed hydrosilylation polymerization of allyldimethylsilane was performed to produce the l-PCS corona. The hydrosilylation mechanism begins with the oxidative addition of the Pt(0) Karstedt's catalyst into the Si−H bond (Figure 1b). Functionalizing the silica nanoparticles with the silane moiety enables the anchoring of the Pt(0) catalyst to the nanoparticle surface. This initial anchoring took approximately 5−10 min and was accompanied by a change in the color of the reaction solution from colorless to yellow. Therefore, when the allyldimethylsilane monomer is subsequently introduced dropwise after the catalyst incubation period, the chains preferentially grow off the silanized Si−H monolayer (Figure 1c). The amount of Karstedt's catalyst added to the reaction vessel corresponded to ~6 catalyst sites/nm^2. Using a substoichiometric amount of catalyst relative to the number of Si−H reaction sites on the silica surface helped facilitate chain growth from the surface of the nanoparticles. As the polymerization proceeded, the reaction media changed color from yellow to dark brown. This color change was significantly slower than in the analogous polymerization in the absence of silica, where the yellow to brown color change was almost immediate. The color change is thought to be associated with the formation of colloidal platinum, a side product of the hydrosilylation reaction.[60] This reduced rate of color change may indicate that the reaction proceeds primarily from the surface as monomer diffuses toward the anchored catalyst sites. The overall concentration of the catalyst is actually higher in the grafting reaction than that of the silica free (solution-based) polymerization of l-PCS, evidence that the reaction rate slows in the presence of silica. This reduced reaction rate necessitated that long polymerization times of 24, 48, and 72 h be employed. Samples from these polymerizations will be referred to as 24-HNP, 48-HNP, and 72-HNP in the remainder of the manuscript.

It was not possible to purify the l-PCS-based HNPs through typical HNP clean-up protocols, such as centrifugation or precipitation into a poor solvent.[59,61,62] The l-PCS-based HNPs dispersed in toluene and toluene/methanol mixtures did not separate into a pellet and supernatant upon centrifugation at 6000−14 000 rpm for 20−40 min. Additionally, our HNPs did not precipitate into mixed solvent systems. Therefore, the HNP materials were removed from their toluene mother liquor and studied without further purification. Dynamic light scattering (DLS) was used to study the sensitivity of the prepared HNPs to free polymer. The addition of free l-PCS at concentrations greater than 5 wt % could be detected by the appearance of an additional peak in the DLS and an increase in the radius of hydration (Figures S9 and S11). We feel that this result provides strong circumstantial evidence that the level of free polymer in our system is rather low.

ATR-FTIR and NMR were used to gain additional insights into the chemical makeup of the HNPs. Spectral features associated with l-PCS from 600 to 1500 cm^{-1} accompany the spectral features from silica in the ATR-FTIR spectra for all of

https://dx.doi.org/10.1021/acs.chemmater.0c00528
Chem. Mater. 2020, 32, 3990−4001

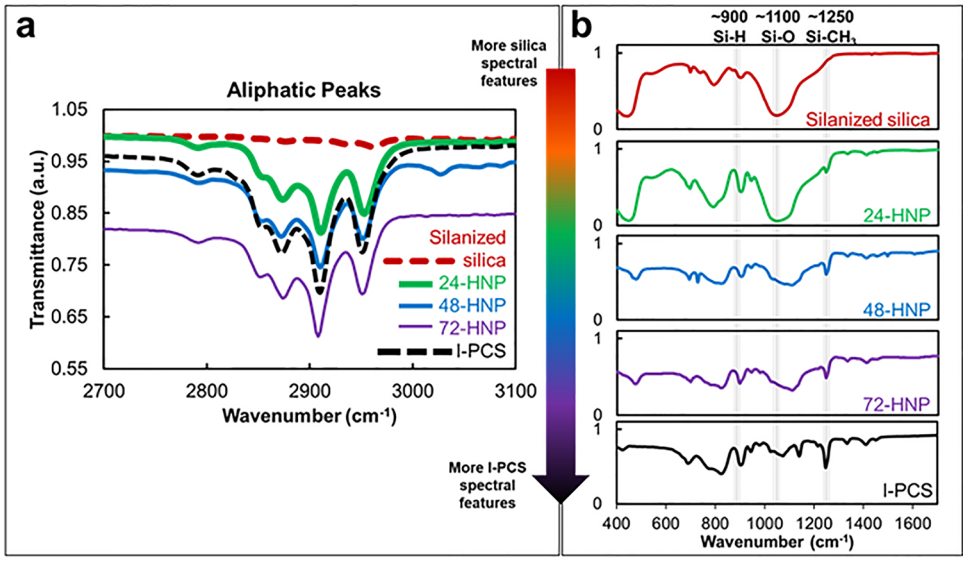

Figure 2. ATR-FTIR spectra of the silanized silica (red), 24-HNP (green), 48-HNP (blue), 72-HNP (purple), and l-PCS (black). The FTIR spectra are split into the aliphatic region (2700−3100 cm^{-1}) (a) and the silane region (400−1700 cm^{-1}) (b). In the aliphatic region (a), the silanized silica spectra are the bold rounded dashed red line, and the l-PCS spectra are the square dashed black line, with the 24-HNP, 48-HNP, and 72-HNP lines ranging in thickness from bold to thin.

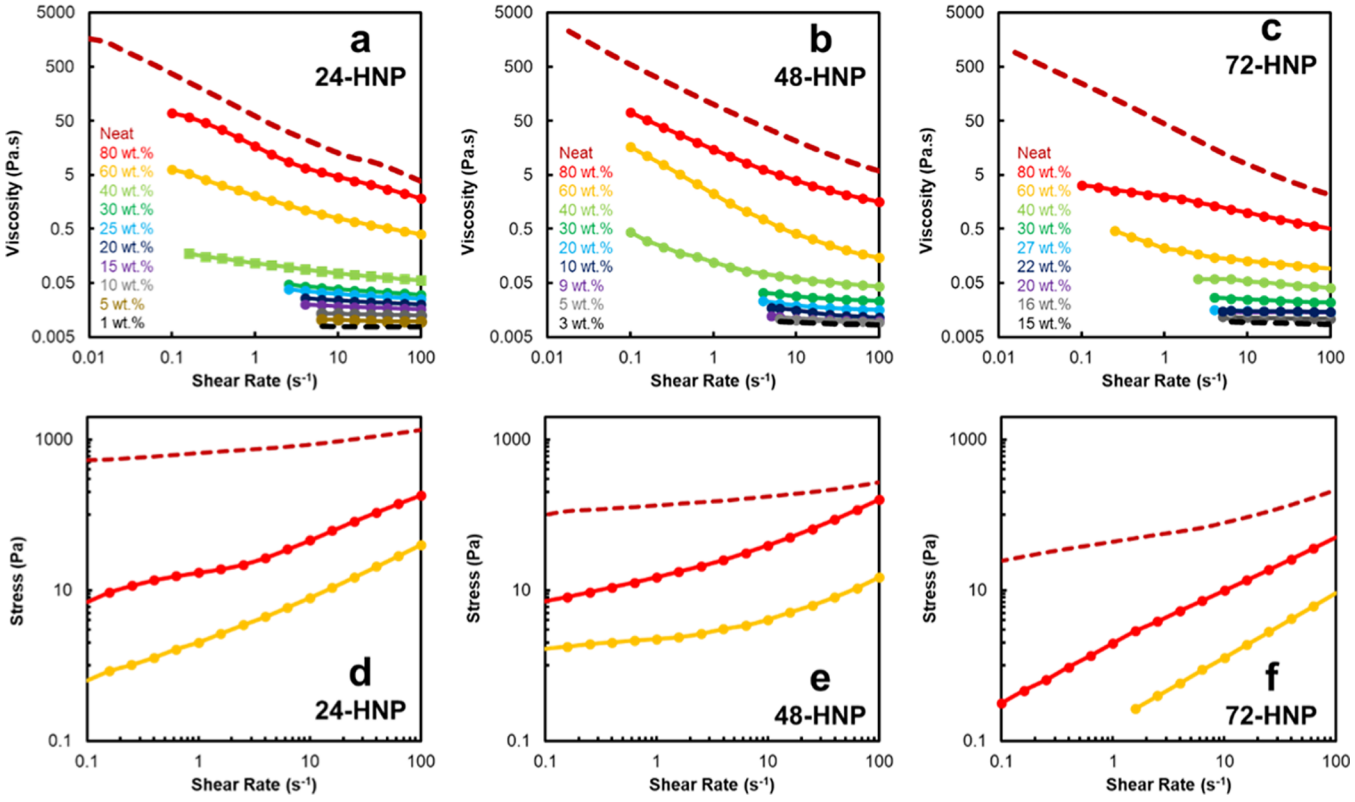

Figure 3. Viscosity profiles of 24-HNP (a), 48-HNP (b), and 72-HNP (c) in the neat state (dark red, top dashed line) and diluted in various weight percents of 2-ethylhexanol. The lowest dilution is represented by the bottom dashed black line for all three samples. The weight percents correspond to core volume fractions (ϕ_c) of ∼0.001−0.1 for the lowest and highest weight percents studied. Stress (Pa) versus shear rate (s^{-1}) for the 24-HNP (d), 48-HNP (e), and 72-HNP (f) in the neat state (dark red, top dashed line) diluted to 80 wt % HNP in 2-ethylhexanol (red) and diluted to 60 wt % HNP in 2-ethylhexanol.

the grafted HNPs (Figure 2b). ATR-FTIR of the grafted HNPs shows strong absorptions in the 2800−3000 cm^{-1} region, indicating that alkyl groups from the polymer are present in the sample (Figure 2a). From the silanized silica spectra (Figure 2a, thick round-dashed red line) to 24-HNP spectra (Figure 2a, thick green line), an increase in the intensities of aliphatic absorptions ∼2800−3000 cm^{-1} is observed. For 24-HNP, the 600−1500 cm^{-1} region is dominated by the Si−O absorption at ∼1100 cm^{-1} with the appearance of the 1250 cm^{-1} $Si-CH_3$ peak (Figure 2b). 48-HNP and 72-HNP samples show more

https://dx.doi.org/10.1021/acs.chemmater.0c00528
Chem. Mater. 2020, 32, 3990−4001

polymer characteristics with a decrease in the Si−O absorption and an increase in the Si−CH_3 peak. ^{1}H NMR was also used to characterize the HNPs, as they were easily dispersible in common organic solvents. ^{1}H NMR shows peaks associated with the 1-PCS repeat unit (Figure S3). This dispersibility provides strong evidence for successful grafting, as the simple physical blending of polymer and SiH-silica nanoparticles did not yield a dispersible system. The HNPs can be considered self-supporting, in that they exhibit viscous flow properties in the absence of solvent. This can be visualized in Figure 1e,f, where 48-HNP and 72-HNP placed on a glass slide flowed down the surface of the slide when it was held vertically (video provided in SI). STEM microscopy of 48-HNP showed a clear corona surrounding the silica cores despite aggregation of the particles due to drying effects (Figure 1g−i).

Steady-State Flow Curves. Viscosity profiling of all HNPS was completed for shear rates ranging from 0.1 to 100 s^{-1} (Figure 3). The samples were either in the neat state or diluted in 2-ethylhexanol by weight. 2-Ethylhexanol was selected for this work as it has a high boiling point (∼186 °C) that reduces the risk of solvent evaporation during the measurements, as well as the high dispersibility of HNPs in this solvent. The samples were diluted from 80 to 1 wt % for 24-HNP (Figure 3a), 80 to 3 wt % for 48-HNP (Figure 3b), and 80 to 15 wt % for 72-HNP (Figure 3c). Below these lower dispersion limits, the viscosity was equivalent to the viscosity of 2-ethylhexanol, indicating full dilution of the particles in the solvent. Qualitatively, the viscosity profiles for the range of dispersions showed similar behaviors across all three HNP samples (24, 48, and 72). The extent of shear thinning was examined by fitting the flow curves with a power law according to the equation $\eta = \gamma^{-m}$, where η is the viscosity, γ is the shear rate, and m is the power law index. Shear-thinning liquids have m values close to unity, while Newtonian liquids have m values below 0.2. A cross-over region exists between 0.3 and 0.7 as materials transition between Newtonian and non-Newtonian behaviors.[63] The plot of m against wt % HNP in 2-ethylhexanol shows a steady increase in m with increasing HNP weight percent (Figure S7), which indicates that the dispersions become more shear thinning as HNP concentration is increased.

At low weight percents, the viscosity is independent of shear rate, demonstrating Newtonian behavior (Figure 3). The HNPs are thermodynamically stable in the 2-ethylhexanol dispersions and do not exhibit any microstructural changes as a result of shear.[64] Newtonian behavior is most clearly exhibited by dispersions between 1 and 30 wt % for 24-HNP, 3 and 30 wt % for 48-HNP, and 15 and 40 wt % for 72-HNP, as shown by m values below 0.2. The viscosities increase with the increasing weight percent of HNPs as higher densities of particles lead to greater numbers of collisions between particles.[65] Regardless, at these weight percents, HNP interactions are infrequent enough that no significant particle network can be formed that would be influenced by shear. This data shows that HNPs can be dispersed at moderate weight percents in 2-ethylhexanol and maintain the fluid flow behaviors of a Newtonian liquid. This indicates that the l-PCS chains are densely grafted, screening the silica−silica interactions that lead to particle aggregation.

Further increasing the weight percent of l-PCS HNPs in 2-ethylhexanol prompts a dependence of viscosity on shear rate, resulting in shear-thinning rheological behavior. At higher weight percents (>30−40%), the particle concentration in the 2-ethylhexanol is sufficient to form loose microstructures, which can be broken with shear, indicated by a decrease in viscosity with higher shear rates.[54] For example, 60−80 wt % dispersions of 24-HNP show an order of magnitude decrease in viscosity from low (0.1 s^{-1}) to high (100 s^{-1}) shear rates (Figure 3a). This indicates that at these concentrations, the interactions between particles began to dominate over the solvent−particle interactions, leading to greater numbers of particle networks. The neat 24-HNP sample shows an approximately 2 orders of magnitude decrease in viscosity with increasing shear rate. In the neat sample, there were no solvent molecules to disperse the HNPs, and the fluid is thus dominated by network formation between brush polymer chains. 48-HNP and 72-HNP follow similar rheological trends as 24-HNP (Figure 3b,c). While there is a dependence of viscosity on shear, all of the neat grafts have m values of ∼0.7, signifying that they are not strongly shear-thinning fluids. This shows that networks formed between neighboring particles are weak and neighboring brushes are most likely not engaging in strong entanglements. This behavior deviates significantly from the rheological properties of l-PCS mixtures with 20 wt % silica physically mixed in (Figure S9). These samples show highly shear-thinning behavior with an m value of 0.84 and a low shear viscosity of approximately 100 000 Pa s (Figure S8).

Figure 3d−f shows the plots of stress (Pa) versus strain rate (s^{-1}) for neat HNPs, as well as HNPs dispersed at 80 and 60 wt % in 2-ethylhexanol. The Herschel−Bulkley equation is used to fit the data to determine yield stress and power law values (Table S2). The neat sample curves show a slight plateau at low strain rates indicating yielding behavior. The highest yield stress is reported for the neat 24-HNP sample at ∼446 Pa, and this value decreases with reaction time. The neat 48-HNP and 72-HNP samples exhibit yield stresses at ∼69 and ∼16 Pa, respectively. The yield stress further decreases with dispersion, and the 80 wt % samples show yield stresses at ∼6, ∼6, and ∼0.07 Pa for the 24-HNP, 48-HNP, and 72-HNP samples, respectively. The plots of the 24-HNP and 48-HNP 80 wt % dispersions show a slight plateauing of the stress−strain curve near low strain rates, while the 72-HNP does not exhibit this behavior. Dispersion to 60 wt % HNP in 2-ethylhexanol furnishes samples with yield stresses at ∼0.6, ∼1.2, and ∼0.06 Pa for the 24-HNP, 48-HNP, and 72-HNP, respectively. The plot of the 48-HNP 60 wt % dispersion displays slight plateauing, while the 24-HNP and 72-HNP samples do not. This data indicates that the neat HNPs require a yield stress to flow, and once flowing, these materials display shear behavior. Dispersing the HNPs in 2-ethylhexanol drastically decreases the yield stress value, indicating that the materials are approaching Newtonian behavior with dispersions of 60 wt % HNPs in the solvent.

To compare the viscosity data to the Krieger−Dougherty (KD) model (eq 1), a frequently used suspension rheology model, the relative shear viscosities (η_r) were plotted against the silica core volume fraction (ϕ_c) for weight fractions ≤40 wt % of the HNPs in 2-ethylhexanol (Figure 4)

$$\eta_r = \left(\frac{1-\phi_c}{\phi_m}\right)^{-\phi_m[\eta]} \quad (1)$$

These fractions were used because the flow curves are more Newtonian and a zero shear viscosity could be accessed. $\eta_r = \eta/\eta_0$, where η is the viscosity of the sample; η_0, the matrix viscosity, is the viscosity of 2-ethylhexanol (0.01 Pa s); and $[\eta]$

https://dx.doi.org/10.1021/acs.chemmater.0c00528
Chem. Mater. 2020, 32, 3990−4001

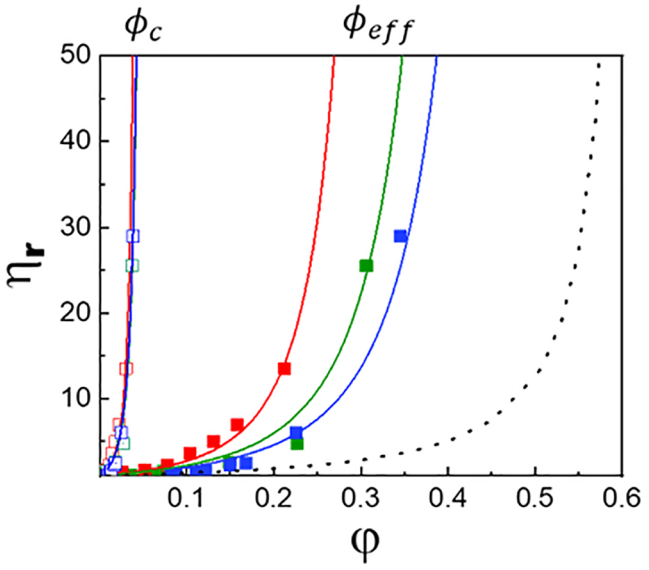

Figure 4. Relative viscosity plotted against ϕ for 24-HNP (red), 48-HNP (green), and 72-HNP (blue). The relative viscosity as a function of silica core volume fraction (ϕ_c) curves is marked by ϕ_c, directly above the curves on the top axis. The relative viscosity as a function of the effective volume fraction (ϕ_{eff}) is marked by ϕ_{eff}, directly above the curves on the top axis, and the dashed line indicates the theoretical hard-sphere behavior calculated from the Krieger–Dougherty (KD) equation. All experimental curves are fit to eq 1 to determine the ϕ_m and $[\eta]$ parameters unique to each curve. The solid lines represent the fits for each data set.

is the intrinsic viscosity. For hard spheres, this value is 2.5. The weight ratios of HNPs dispersed in 2-ethylhexanol were first converted to silica core volume fractions by the following equation2

$$\phi_c = \frac{\rho\phi_w}{1 + (\rho - 1)\phi_w} \tag{2}$$

where ρ indicates the ratio of the polycarbosilane density to that of SiO_2, and ϕ_w is the weight fraction of silica in the dispersion, determined through TGA (Figure S5).

For all three grafted samples, the relative shear viscosities rapidly increase at low core volumes (Figure 4), deviating significantly from the standard hard-sphere behavior, as defined by the Krieger–Dougherty relationship (dashed black line, Figure 4). In the Krieger–Dougherty relationship, the maximum packing volume fraction of hard spheres in a matrix is 0.63, and viscosity becomes infinitely large near this core volume fraction. This is the relationship that would apply in the case of an aqueous dispersion of isotropic, rigid latex spheres.[66] However, for 24-, 48-, and 72-HNPs, the relative viscosities rapidly increase at much lower core volumes than 0.63. Fitting these curves to eq 1 provides a realization of ϕ_m and $[\eta]$ for the HNP relative viscosities as a function of silica core volume fraction (Table 1). The maximum packing volume fraction for all three HNP samples is ~0.06–0.07. The inverse of the intrinsic viscosity is equivalent to the overlap volume fraction, ϕ^*, and this value is ~25 times smaller than the typical hard-sphere suspension.[67] This behavior indicates that both the polymer corona and silica sphere contribute to an effective core volume, ϕ_{eff}, as follows[64,68]

$$\phi_{eff} = \phi_c\left(1 + \frac{L}{a_c}\right)^3 \tag{3}$$

For these samples, the silica particle radius, a_c, was set to be 7.5 nm, as the diameter of the silica spheres ranges from 10 to 20 nm. L is the brush length of the grafted polymer, and brush lengths were determined through dynamic light scattering, giving values of 6.89 ± 2.34, 7.65 ± 1.38, and 8.14 ± 0.88 nm for 24-HNP, 48-HNP, and 72-HNP, respectively (Figure S4).

Knowing the brush length allows for a more accurate representation of relative shear viscosity as a function of volume core. The relative viscosities plotted against the effective core volume show behavior closer to that of the standard hard-sphere behavior, indicating that the polymer brush augments the silica core to some extent (Figure 4). However, for all samples, the viscosities deviate at lower fractions than a standard hard-sphere system. Parameters ϕ_m and $[\eta]$ are also determined for the relative viscosities as a function of ϕ_{eff} for all three HNP samples (Table 1). The maximum packing volume fraction for the 24-HNP sample is ~0.39, and this value increases with reaction time to 0.56 and 0.59 for the 48-HNP and 72-HNP samples, respectively. The overlap volume fractions are 2.5–3.6 times smaller than for a typical hard-sphere suspension. Since the onset of jamming for all samples is still lower than 0.63, this may indicate that the HNPs are forming loose networks in the solvent at the weight percents where jamming occurs, increasing the relative viscosity at lower core volumes than the theoretical max packing fraction.[69] The propensity for the HNPs to form networks could be influenced by unscreened silica–silica interactions, polymer brush interactions with neighboring particles, and brush–solvent interactions. Additionally, the length of the brush and grafting density can also impact network formation in solvated HNP systems.[70] For our HNP system, it is clear that the brush length impacts the concentration in which jamming occurs, with longer brush lengths shifting jamming to higher concentrations. However, the mechanism driving the network formation of these HNPs is still being determined.

Significantly, the grafting of l-PCS from the SiO_2 surface enables these nanoparticles to be included in a preceramic polymer matrix at relatively high concentrations. Further, the

Table 1. ϕ_m and $[\eta]$ Parameters Determined through Fitting Relative Viscosity as a Function of Silica Core Volume Fraction (ϕ_c) and as a Function of Effective Volume Fraction (ϕ_{eff})[a]

	KD fitting from ϕ_c			KD fitting from ϕ_{eff}		
	ϕ_m	$[\eta]$	ϕ^*	ϕ_m	$[\eta]$	ϕ^*
24-HNP	0.06 ± 0.0009	61.7 ± 1.7	0.016	0.39 ± 0.007	8.7 ± 0.24	0.11
48-HNP	0.07 ± 0.001	59.7 ± 1.5	0.017	0.56 ± 0.008	7.3 ± 0.19	0.14
72-HNP	0.07 ± 0.001	60.9 ± 1.1	0.016	0.59 ± 0.08	6.38 ± 1.1	0.16

[a] ϕ^* values determined from the inverse of $[\eta]$.

https://dx.doi.org/10.1021/acs.chemmater.0c00528
Chem. Mater. 2020, 32, 3990–4001

addition of these HNPs should confer improved weight retention and limit shrinkage upon pyrolysis, while not radically disturbing the rheological characteristics of the polymer. Applications such as PIP processing, which requires preceramic polymers to flow into the pores of a ceramic piece, would benefit from the combined relatively low viscosity and high solid loadings of these new preceramic hybrid HNPs.

Thermal Transitions Associated with Preceramic HNPs. Prior to examining the thermal transitions of preceramic HNPs, untethered l-PCS (8 kDa) was examined via DSC. As seen in Figure 5, l-PCS (black trace) exhibits a melting transition near 13 °C. When examining the thermal transitions of semicrystalline polymers, the number of melting transitions is indicative of the number of chain-packing configurations present in the crystallite.[71,72] Additionally, shifts in melting transitions of a polymer directly correspond to changes in the crystalline structure.[71,72] Therefore, the single melting transition displayed by l-PCS indicates the presence of a single crystalline domain. This result aligns with a previous report by Tsyba, who concluded that l-PCS orients in a single, fully extended chain-packing configuration.[73] However, it is worth noting that both the melting temperature and the number of melting transitions observed herein for l-PCS deviate from a previous investigation examining the properties of l-PCS synthesized via anionic polymerization.[74] Specifically, Isono et al. reported that l-PCS polymers having $M_n > 10^5$ exhibit multiple melting transitions near 37 °C. Discrepancies in the melting point temperature and the number of transitions are attributed to differences in molecular weight. For example, Qiu et al. reported that increasing the molecular weight of semicrystalline polymers increased both the melting point temperature and the number of crystalline domains.[75] Moreover, Qiu et al. concluded that most low-molecular-weight semicrystalline polymers exhibit one melting transition (extended chain-packing configuration).[75] Further, these authors noted that increasing the molecular weight increases the number of chain-packing configurations ranging from extended to once-folded, twice-folded, and thrice-folded.[75] Thus, with the low-molecular-weight l-PCS utilized here, it is reasonable to suspect that the melting transitions observed at 13 °C are due to crystalline domains having an extended chain-packing configuration.

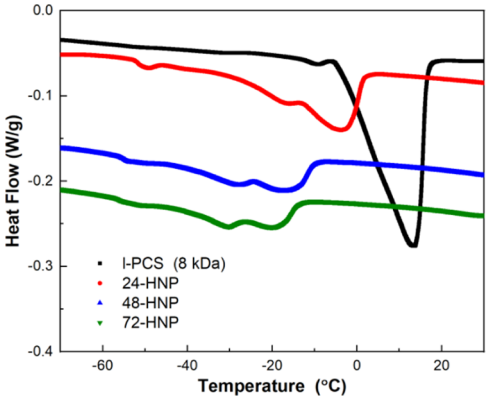

Figure 5. DSC results display the thermal transitions of l-PCS and HNP samples. Displayed DSC traces were obtained on the second heating curve of a heat−cool−heat cycle at 10 °C from −80 to 80 °C.

In addition to untethered l-PCS, Figure 5 also displays DSC results for all HNP samples. Three main observations can be deduced from these results. First, all HNP samples display a decrease in the intensity of the melting point compared to l-PCS. This indicates that tethering l-PCS to silica particles hinders the formation of crystalline l-PCS domains and decreases the amount of crystalline phase present in the self-suspended HNP.[76] Moreover, the enthalpy of melting for HNP samples is significantly lower than the enthalpy of melting observed in l-PCS, as seen in Table S1, indicating that the rate of crystallization is lower in HNP samples than in l-PCS samples. The enthalpy of melting of 100% crystalline l-PCS has not been reported in the literature, making it impossible for us to quantify the percent of crystallinity for our HNPs. However, we can consider prior l-PCS results and make inferences with previous studies examining poly(ethylene oxide) (PEO) nanocomposites. For example, Burgaz reported that both the melting peak intensity and enthalpy of melting in PEO nanocomposites decrease as the loading level of clay and fumed silica increases.[76] Burgaz attributed these results to the presence of clay and fumed silica, which limit crystallization. Second, all HNP samples display a decrease in the peak melting point and crystallization temperature as compared to l-PCS, with the decrease corresponding to increasing reaction time (Figures 5 and S6). As suggested by Kumar et al., depressions in crystallization temperatures for polymer nanocomposites indicate that nanofillers are unable to nucleate

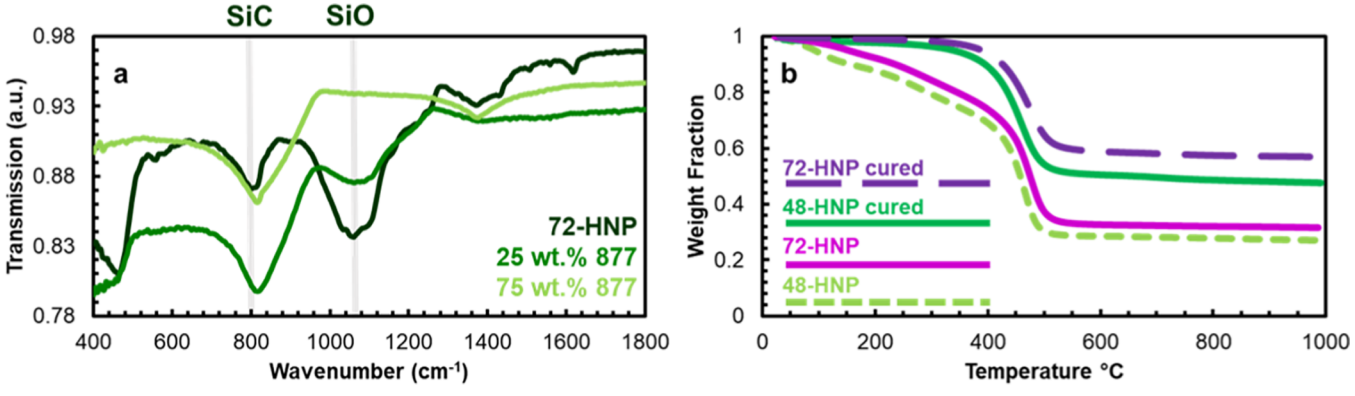

Figure 6. (a) ATR-FTIR of neat HNP and composites pyrolyzed at 1000 °C. 72-HNP shows both SiC and SiO absorptions, while increasing the wt % of SMP-877, SiC absorptions become more prominent. (b) TGA curves of 48-HNP (dashed light green line), 72-HNP (magenta line), cured 48-HNP (green line), and cured 72-HNP (large dashed purple line).

https://dx.doi.org/10.1021/acs.chemmater.0c00528
Chem. Mater. 2020, 32, 3990−4001

polymer chains since nucleation generally increases both the melting and crystallization temperatures.[77] Thus, the decrease observed in the peak melting point and crystallization temperature suggests that nucleation plays an inconsequential role in the thermal transitions of self-suspended HNPs. This strengthens our previous inference that suggested that grafting alters the growth of crystalline domains and rate of crystallization in self-suspended HNPs. Finally, all HNP samples display a broadening and an increase in the number of melting transitions. As alluded to previously, the number of melting transitions corresponds to the number of chain-packing configurations present in the crystallite.[72,78] Thus, the appearance of new melting transitions in the HNP samples suggests that new crystalline domains containing different chain-packing configurations are present. While beyond the scope of the current investigation, this result is striking and has prompted additional studies examining the hierarchical structure of l-PCS grafted to spherical nanoparticles.

Conversion of HNPs and HNP/Preceramic Polymer Mixtures to Ceramics. The conversion efficiency of HNPs to purely ceramic systems was assessed using thermal gravimetric analysis (TGA) to determine the fraction of mass retained upon heating to 1000 °C. For HNP samples tested as synthesized (i.e., were not cured prior to pyrolysis), the polymer brush is completely lost between 400 and 500 °C, leaving pure silica (determined through XRD). Thermally curing the HNPs for 1 h at 160 °C followed by another hour at 250 °C under vacuum improved the ceramic yield at 1000 °C by 20−25% and converted the brush to silicon carbide, giving a total ceramic yield of ∼60% (Figure 6). In all samples, the first thermal loss occurred from 0 to 200 °C and constitutes 5−8% of the sample weight. This was attributed to the loss of adsorbed water or solvent from the sample. The loss of organic groups from the polymer brush occurs from 400 to 500 °C. The remaining material, whether pure silica or silicon carbide, was thermally resistant, and no more weight loss occurred up to 1000 °C. While our current work provides a proof of principle, in future research, we plan to further improve the ceramic yield by altering the architecture of the preceramic polymer corona to a macromolecule that is more optimized for ceramic conversion.

Formulations of HNPs and SMP-877 (a commercially available polycarbosilane) were made to study the ceramic composition with additional preceramic polymer present in the sample. As we anticipate that HNPs can be used in combination with commercial preceramic polymers to create customized formulations, we undertook a short study to determine the conversion behavior of these mixed systems. The mixed HNP/SMP-877 samples were thermally cross-linked before and pyrolyzed to 1400 °C for 1 h in a graphite furnace. ATR-FTIR was used to examine the chemical structure of the cross-linked (neat) 72-HNP and HNP/SMP-877 materials after pyrolysis (Figure 6). The major absorptions appearing at 1066 and 819 cm^{-1} corresponded to Si−O bonds and Si−C bonds, respectively. Additionally, some carbon was present in the neat pyrolyzed HNP sample, exhibiting absorptions at ∼1600 and ∼2900 cm^{-1}. With increasing weight ratio of SMP-877 in the pyrolyzed material, the intensity of the Si−C absorption increases, while the Si−O absorption decreases. As expected, this indicates a greater concentration of silicon carbide in the composite as opposed to silica, corresponding to a greater concentration of SiC-converting material in the prepyrolyzed sample. Characterization of HNP- and HNP/SMP-877-derived materials by X-ray diffraction indicated the presence of similar crystalline phases, independent of the sample (Figure 7). The neat

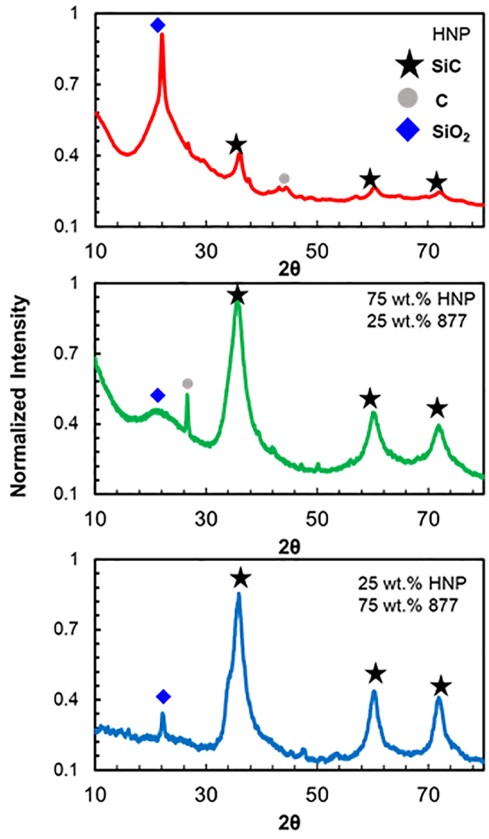

Figure 7. XRD spectra of HNP pyrolyzed at 1400 °C (top curve) showing conversion to SiC in addition to SiO_2 from the silica core. Increasing the amount of SMP-877 (middle and bottom curves) increased the SiC intensities compared to that of the SiO_2 intensities.

pyrolyzed HNP sample showed β-SiC at 2θ values of 36, 60, and 72°. Additionally, the largest intensity peak at 22° is associated with SiO_2 domains, and small intensity carbon peaks were also observed at ∼44°. The HNP/SMP-877-derived composites show spectra dominated by SiC, with minor SiO_2 features. This data agreed with the ATR-FTIR spectra and showed that SiC was formed from the pyrolysis of cured HNPs. Further, this data qualitatively shows that the SiC content can be increased by increasing the proportion of polycarbosilane in the system, through the addition of exogenous preceramic polymer (e.g., SMP-877).

CONCLUSIONS

As detailed in this manuscript, we have succeeded in synthesizing solvent-free and free-flowing HNP liquids utilizing polymer brushes that are novel in both their chemistry and functionality. These first examples of preceramic polymer-grafted HNPs were synthesized by growing l-PCS (using hydrosilylation chemistry) from the functionalized surface of silica nanoparticles. Conformation of the synthesis of these new HNPs by chemistry that is both facile and well defined was verified through ATR-FTIR and ^1H NMR, and TEM characterization. The HNPs produced through this grafting method are self-supporting viscous fluids that can flow with an applied force (e.g., under the influence of gravity). Addition-

https://dx.doi.org/10.1021/acs.chemmater.0c00528
Chem. Mater. 2020, 32, 3990−4001

ally, these HNPs are easily dispersible in a variety of common organic solvents such as toluene, dichloromethane, and chloroform. Rheological data provided quantitative information on the flow properties of neat HNPs, as well as HNPs dispersed in an organic solvent. In addition to the unique rheological properties conferred by the grafting of l-PCS to nanoparticles, these polymer chains may also be converted to SiC after thermal curing with reasonable ceramic yields at 1000 °C. Formulations of HNPs with commercial preceramic polymers were investigated and found to be a utilitarian strategy to tailor the amount of SiC in the final ceramic nanocomposite. The straightforward synthesis of SiC-converting HNPs that we have described provides a useful scientific platform for studying the physical properties of preceramic polymer/nanoparticle hybrids. Additionally, we anticipate that this new class of preceramic polymer-based HNPs will provide significant technological advantages, including the ability to create nanocomposites with exquisitely controlled nanostructures. Further, the unique hybrid architecture of these materials could allow one to access nanocomposite compositions that are not obtainable through purely polymer-derived strategies. In considering the prior work and multitude of materials explored in both the HNP and preceramic polymer chemistry fields, we anticipate that this new class of nanoparticles will pave the way for a substantial and diverse family of hybrids.

■ ASSOCIATED CONTENT

Supporting Information

The Supporting Information is available free of charge at https://pubs.acs.org/doi/10.1021/acs.chemmater.0c00528.

Additional ATR-FTIR of bare and silanized silica particles, TGA profile of silanized silica, grafting density calculations, ^{1}H NMR (l-PCS, 72 h HNPs, 48 h HNPs, and 24 h HNPS), correlation function curves to find HNP radii, TGA curve of uncured HNPs, DSC thermogram displaying the crystallization peaks, enthalpy of melting values determined from DSC thermograms, power law fit of viscosity curves for the three HNP samples, viscosity profile of 20 wt % silica mixed into l-PCS, dynamic light scattering of 72-HNP mixed with different weight percents of free l-PCS, DLS size profile of neat 72-HNPs, radius of hydration (nm) plotted against the weight fraction of added free 1-PCS, table of shear stress (Pa) and power law values determined through the Herschel−Bulkley relationship, table of weight percents of HNP dispersed in 2-ethylhexanol and corresponding ϕ_c and ϕ_{eff} values, plot of viscosity for the 48-HNP at different gap heights, viscosity at different gap heights for selected shear rates, and normalized shear stress plotted against gap height for selected shear rates (PDF)

Video showing flow down of 72-HNP in 10× speed in the absence of solvent (AVI)

■ AUTHOR INFORMATION

Corresponding Author

Matthew B. Dickerson − *Materials and Manufacturing Directorate, Air Force Research Laboratory, Wright-Patterson AFB, Ohio 45433, United States;* orcid.org/0000-0003-3000-0290; Email: matthew.dickerson.6@us.af.mil

Authors

Kara L. Martin − *Materials and Manufacturing Directorate, Air Force Research Laboratory, Wright-Patterson AFB, Ohio 45433, United States; UES, Inc., Dayton, Ohio 45432, United States*

Dayton P. Street − *Materials and Manufacturing Directorate, Air Force Research Laboratory, Wright-Patterson AFB, Ohio 45433, United States; NRC Research Associateship Programs, The National Academies, Washington, District of Columbia 20001, United States;* orcid.org/0000-0003-2505-7137

Complete contact information is available at: https://pubs.acs.org/10.1021/acs.chemmater.0c00528

Notes

The authors declare no competing financial interest.

■ ACKNOWLEDGMENTS

The authors acknowledge support from the Air Force Research Laboratory Materials &Manufacturing Directorate, and the Air Force Office of Scientific Research under the Low Density Materials/Aerospace Composites Portfolio, program officers Drs. Jay Tiley and Ming-Jen Pan. This research was performed while the author (D.P.S.) held an NRC Research Associateship award at the Air Force Research Laboratory. The authors are grateful to Dr. Hilmar Koerner (AFRL) and Prof. Subramanian Ramakrishnan (FAMU-FSU) for helpful discussions. K.L.M. and M.B.D. have filed a patent application of the technology presented in this article. The views expressed are those of the authors and do not reflect the official policy or position of the U.S. Air Force, Department of Defense, or the U.S. Government. Distribution A. Approved for public release: distribution unlimited 88ABW-2020-1150.

■ REFERENCES

(1) Colombo, P.; Mera, G.; Riedel, R.; Soraru, G. D. Polymer-Derived Ceramics: 40 Years of Research and Innovation in Advanced Ceramics. *J. Am. Ceram. Soc.* **2010**, *93*, 1805−1837.

(2) Rittscher, V.; Gallei, M. A convenient synthesis strategy for microphase-separating functional copolymers: the cyclohydrocarbosilane tool box. *Polym. Chem.* **2015**, *6*, 5653−5662.

(3) Piriou, C.; Viers, L.; Lucas, R.; Bouzat, F.; Laadoua, H.; Champavier, Y.; Foucaud, S.; Coelho, C.; Babonneau, F. Rheological and thermal behaviours of a hyperbranched polycarbosilanes. *Appl. Organomet. Chem.* **2018**, *32*, No. e4443.

(4) Han, M.; Yin, X.; Duan, W.; Ren, S.; Zhang, L.; Cheng, L. Hierarchical graphene/SiC nanowire networks in polymer-derived ceramics with enhanced electromagnetic wave absorbing capability. *J. Eur. Ceram. Soc.* **2016**, *36*, 2695−2703.

(5) Ngoumeni-Yappi, R.; Fasel, C.; Riedel, R.; Ischenko, V.; Pippel, E.; Woltersdorf, J.; Clade, J. Tuning of the Rheological Properties and Thermal Behavior of Boron-Containing Polysiloxanes. *Chem. Mater.* **2008**, *20*, 3601−3608.

(6) Wilfert, J.; von Hagen, R.; Fiz, R.; Jansen, M.; Mathur, S. Electrospinning of preceramic polymers for the preparation of SiBNC felts and their modification with semiconductor nanowires. *J. Mater. Chem.* **2012**, *22*, 2099.

(7) Sorarù, G. D.; Dalcanale, F.; Campostrini, R.; Gaston, A.; Blum, Y.; Carturanc, S.; Aravind, P. R. Novel polysiloxane and polycarbosilane aerogels via hydrosilylation of preceramic polymers. *J. Mater. Chem.* **2012**, *22*, 7676.

(8) Zheng, N.; Hou, J.; Zhao, H.; Wu, J.; Luo, Y.; Bai, H.; Rogers, J. A.; Zhao, Q.; Xie, T. Mechano-Plastic Pyrolysis of Dynamic Covalent Polymer Network toward Hierarchical 3D Ceramics. *Adv. Mater.* **2019**, *31*, No. 1807326.

(9) Rueschhoff, L. M.; Baldwin, L. A.; Wheeler, R.; Dalton, M. J.; Koerner, H.; Berrigan, J. D.; Bedford, N. M.; Seifert, S.; Cinibulk, M. K.; Dickerson, M. B. Fabricating Ceramic Nanostructures with Ductile-like Compression Behavior via Rapid Self-Assembly of Block Copolymer and Preceramic Polymer Blends. *ACS Appl. Nano Mater.* **2019**, *2*, 250−257.
(10) Colombo, P.; Soraru, G. D.; Riedel, R.; Kleebe, H. *Polymer Derived Ceramics: From Nano-Structure to Applications*; DEStech Publications, Inc.: Lancaster, Pennsylvannia 17692, 2010; Vol. *410*.
(11) Wei, D.; Chen, L.; Xu, T.; He, W.; Wang, Y. Synthesis and Characterization of a Novel Borazine-Type UV Photo-Induced Polymerization of Ceramic Precursors. *Molecules* **2016**, *21*, No. 801.
(12) Ly, H. Q.; Taylor, R.; Day, R. J.; Heatley, F. Conversion of polycarbosilane (PCS) to SiC-based ceramic Part 1. Characterisation of PCS and curing products. *J. Mater. Sci.* **2001**, *36*, 4037−4043.
(13) Tong, D.; Wang, H.; Chen, L.; Wang, L.; Li, Z. A novel carborane-containing ceramic precursor: Synthesis, characterization, and ceramic conversion mechanism. *High Perform. Polym.* **2019**, *31*, 694−706.
(14) Will, U.; Veljanovski, D.; Härter, P.; Rieger, B. Hyperbranched Polycarbosilanes of Homogeneous Architecture: Regioselective Hydrosilylation of AB2Monomers and Consecutive Functionalization. *Macromolecules* **2010**, *43*, 934−938.
(15) Zhang, G.-B.; Kong, J.; Fan, X.-D.; Li, X.-G.; Tian, W.; Huang, M.-R. UV-activated hydrosilylation: a facile approach for synthesis of hyperbranched polycarbosilanes. *Appl. Organomet. Chem.* **2009**, *23*, 277−282.
(16) Ji, P.; Pei, X.; Miao, Y.; He, L.; Huang, Q. Effect of ultraviolet irradiation on the cross-linking process and ceramic yield of liquid hyperbranched polycarbosilane. *Adv. Appl. Ceram.* **2017**, *116*, 445−451.
(17) Huang, Y.; Liu, L.; Zhang, S.; Yu, H.; Yang, J. Polycarbosilane-modified styrene-based polymers with ultra-low dielectric constant, greatly enhanced mechanical strength and thermal stability. *Eur. Polym. J.* **2018**, *98*, 347−353.
(18) Gallei, M.; Li, J.; Elbert, J.; Mazurowski, M.; Schönberger, A.; Schmidt, C.; Stühn, B.; Rehahn, M. Immobilization of Poly(1,1-dimethysilacyclobutane) by Means of Anionic Ring-Opening Polymerization on Organic Nanoparticles and Reinvestigation of Crystallization. *Polymers* **2013**, *5*, 284−302.
(19) Elbert, J.; Didzoleit, H.; Fasel, C.; Ionescu, E.; Riedel, R.; Stühn, B.; Gallei, M. Surface-Initiated Anionic Polymerization of [1]Silaferrocenophanes for the Preparation of Colloidal Preceramic Materials. *Macromol. Rapid Commun.* **2015**, *36*, 597−603.
(20) Scheffler, M.; Bordia, R.; Travitzky, N.; Greil, P. Development of a rapid crosslinking preceramic polymer system. *J. Eur. Ceram. Soc.* **2005**, *25*, 175−180.
(21) Mera, G.; Gallei, M.; Bernard, S.; Ionescu, E. Ceramic Nanocomposites from Tailor-Made Preceramic Polymers. *Nanomaterials* **2015**, *5*, 468−540.
(22) He, W.; Chen, L.; Peng, F. Coating formed by SiBCN single source precursor via UV-photopolymerization. *Mater. Lett.* **2017**, *206*, 121−123.
(23) Baldwin, L. A.; Rueschhoff, L. M.; Deneault, J. R.; Cissel, K. S.; Nikolaev, P.; Cinibulk, M. K.; Koerner, H.; Dalton, M. J.; Dickerson, M. B. Synthesis of a Two-Component Carbosilane System for the Advanced Manufacturing of Polymer-Derived Ceramics. *Chem. Mater.* **2018**, *30*, 7527−7534.
(24) Eckel, Z. C.; Zhou, C.; Martin, J. H.; Jacobsen, A. J.; Carter, W. B.; Schaedler, T. A. Additive Manufacturing of Polymer-Derived Ceramics. *Science* **2016**, *351*, 58−62.
(25) Zanchetta, E.; Cattaldo, M.; Franchin, G.; Schwentenwein, M.; Homa, J.; Brusatin, G.; Colombo, P. Stereolithography of SiOC Ceramic Microcomponents. *Adv. Mater.* **2015**, *28*, 370−376.
(26) Greil, P. Polymer Derived Engineering Ceramics. *Adv. Eng. Mater.* **2000**, *2*, 339−348.
(27) Hasegawa, Y.; Iimura, M.; Yajima, S. Synthesis of Continuous Silicon Carbide Fibers. *J. Mater. Sci.* **1980**, *15*, 720−728.
(28) Ishikawa, T.; Kohtoku, Y.; Kumagawa, K.; Tamamura, T.; Nagasawa, T. High-strength alkali-resistant sintered SiC fibre stable to 2,200 °C. *Nature* **1998**, *391*, 773−775.
(29) Lewinsohn, C. A.; Colombo, P.; Reimanis, I.; Unal, O. Stresses Occurring During Joining of Ceramics Using Preceramic Polymers. *J. Am. Ceram. Soc.* **2001**, *84*, 2240−2244.
(30) Zhong, X.; Pei, X.; Miao, Y.; He, L.; Huang, Q. Accelerating the crosslinking process of hyperbranched polycarbosilane by UV irradiation. *J. Eur. Ceram. Soc.* **2017**, *37*, 3263−3270.
(31) Blum, Y. D.; Schwartz, K. B.; Laine, R. M. Preceramic polymer pyrolysis Part 1 Pyrolytic properties of polysilazanes. *J. Mater. Sci.* **1989**, *24*, 1707−1718.
(32) Takeda, M.; Kagawa, Y.; Mitsuno, S.; Imai, Y.; Ichikawa, H. Strength of a Hi-Nicalon/Silicon-Carbide-Matrix Composite Fabricated by the Multiple Polymer Infiltration−Pyrolysis Process. *J. Am. Ceram. Soc.* **1999**, *82*, 1579−1581.
(33) Gudapati, V. M.; Veedu, V. P.; Ghasemi-Nejhad, M. N. Polymeric precursor pyrolysis for flexural property evaluation of continuous fiber ceramic nanocomposites with nanoparticles. *Compos. Sci. Technol.* **2006**, *66*, 3230−3240.
(34) Suttor, D.; Kleebe, H.-J.; Ziegler, G. Formation of Mullite from Filled Siloxanes. *J. Am. Ceram. Soc.* **1997**, *80*, 2541−2548.
(35) Gorjan, L.; Tonello, R.; Sebastian, T.; Colombo, P.; Clemens, F. Fused deposition modeling of mullite structures from a preceramic polymer and γ-alumina. *J. Eur. Ceram. Soc.* **2019**, *39*, 2463−2471.
(36) Greil, P. Active-filler-controlled pyrolysis of preceramic polymers. *J. Am. Ceram. Soc.* **1995**, *78*, 835−848.
(37) Colombo, P.; Bernardo, E.; Parcianello, G. Multifunctional advanced ceramics from preceramic polymers and nano-sized active fillers. *J. Eur. Ceram. Soc.* **2013**, *33*, 453−469.
(38) Suri, P.; Atre, S. V.; German, R. M.; de Souza, J. P. Effect of mixing on the rheology and particle characteristics of tungsten-based powder injection molding feedstock. *Mater. Sci. Eng., A* **2003**, *356*, 337−344.
(39) Wang, H.; Zeng, C.; Elkovitch, M.; Lee, L. J.; Koelling, K. W. Processing and Properties of Polymeric Nano-Composites. *Polym. Eng. Sci.* **2001**, *41*, 2036−2046.
(40) Xavier, P.; Rao, P.; Bose, S. Nanoparticle induced miscibility in LCST polymer blends: critically assessing the enthalpic and entropic effects. *Phys. Chem. Chem. Phys.* **2016**, *18*, 47−64.
(41) Pryamitsyn, V.; Ganesan, V. Mechanisms of steady-shear rheology in polymer-nanoparticle composites. *J. Rheol.* **2006**, *50*, 655.
(42) Willenbacher, N.; Georgieva, K. Rheology of Disperse Systems. In *Product Design and Engineering: Formulation of Gels and Pastes*;Brockel, U.; Meier, W.; Wagner, G., Eds.; Wiley-VCH Verlag GmbH & Co.: Weinheim, Germany, 2013.
(43) Zoli, L.; Sciti, D. Efficacy of a ZrB2−SiC matrix in protecting C fibres from oxidation in novel UHTCMC materials. *Mater. Des.* **2017**, *113*, 207−213.
(44) Ndong, R. S.; Russel, W. B. Effects of molecular weight and volume fraction on rheological properties of PDMS-grafted alumina in PDMS melts. *J. Rheol.* **2011**, *55*, 331−351.
(45) Fernandes, N. J.; Koerner, H.; Giannelis, E. P.; Vaia, R. A. Hairy nanoparticle assemblies as one-component functional polymer nanocomposites: opportunities and challenges. *MRS Commun.* **2013**, *3*, 13−29.
(46) Salami-Kalajahi, M.; Haddadi-Asl, V.; Behboodi-Sadabad, F.; Rahimi-Razin, S.; Roghani-Mamaqani, H. Properties of PMMA/Carbon Nanotubes Nanocomposites Prepared by "Grafting Through" Method. *Polym. Compos.* **2012**, *33*, 215−224.
(47) Poling-Skutvik, R.; Slim, A. H.; Narayanan, S.; Conrad, J. C.; Krishnamoorti, R. Soft interactions modify the diffusive dynamics of polymer-grafted nanoparticles in solutions of free polymer. *ACS Macro Lett.* **2019**, *8*, 917−922.
(48) Jiao, Y.; Tibbits, A.; Gillman, A.; Hsiao, M.-S.; Buskohl, P.; Drummy, L. F.; Vaia, R. A. Deformation Behavior of Polystyrene-Grafted Nanoparticle Assemblies with Low Grafting Density. *Macromolecules* **2018**, *51*, 7257−7265.

https://dx.doi.org/10.1021/acs.chemmater.0c00528
Chem. Mater. 2020, 32, 3990−4001

(49) Sunday, D. F.; Green, D. L. Thermal and Rheological Behavior of Polymer Grafted Nanoparticles. *Macromolecules* **2015**, *48*, 8651−8659.
(50) Sunday, D. F.; Ilavsky, J.; Green, D. L. A Phase Diagram for Polymer-Grafted Nanoparticles in Homopolymer Matrices. *Macromolecules* **2012**, *45*, 4007−4011.
(51) Tchoul, M. N.; Fillery, S. P.; Koerner, H.; Drummy, L. F.; Oyerokun, F. T.; Mirau, P. A.; Durstock, M. F.; Vaia, R. A. Assemblies of Titanium Dioxide-Polystyrene Hybrid Nanoparticles for Dielectric Applications. *Chem. Mater.* **2010**, *22*, 1749−1759.
(52) Lenart, W. R.; Hore, M. J. A. Structure−property relationships of polymer-grafted nanospheres for designing advanced nanocomposites. *Nano-Struct. Nano-Objects* **2018**, *16*, 428−440.
(53) Chevigny, C.; Dalmas, F.; Di Cola, E.; Gigmes, D.; Bertin, D.; Boué, F.; Jestin, J. Polymer-Grafted-Nanoparticles Nanocomposites: Dispersion, Grafted Chain Conformation, and Rheological Behavior. *Macromolecules* **2011**, *44*, 122−133.
(54) Liu, J.; Cheng, Y.; Xu, K.; An, L.; Su, Y.; Li, X.; Zhang, Z. Effect of nano-silica filler on microstructure and mechanical properties of polydimethylsiloxane-based nanocomposites prepared by "inhibition-grafting" method. *Compos. Sci. Technol.* **2018**, *167*, 355−363.
(55) Bai, L.; Bai, Y.; Zheng, J. Improving the filler dispersion and performance of silicone rubber/multi-walled carbon nanotube composites by noncovalent functionalization of polymethylphenylsiloxane. *J. Mater. Sci.* **2017**, *52*, 7516−7529.
(56) Vowinkel, S.; Boehm, A.; Schäfer, T.; Gutmann, T.; Ionescu, E.; Gallei, M. Preceramic core-shell particles for the preparation of hybrid colloidal crystal films by melt-shear organization and conversion into porous ceramics. *Mater. Des.* **2018**, *160*, 926−935.
(57) Choueiri, R. M.; Klinkova, A.; Pearce, S.; Manners, I.; Kumacheva, E. Self-Assembly and Surface Patterning of Polyferrocenylsilane-Functionalized Gold Nanoparticles. *Macromol. Rapid Commun.* **2018**, *39*, No. 1700554.
(58) Dasan, A.; Lucas, R.; Laborde, E.; Piriou, C.; Foucaud, S. Towards a surface functionalisation and grafting of a polycarbosilane onto zirconium carbide particles for the development of hybrid core-shell structures. *Appl. Surf. Sci.* **2019**, *495*, No. 143409.
(59) Bentz, K. C.; Savin, D. A. Chain Dispersity Effects on Brush Properties of Surface-Grafted Polycaprolactone-Modified Silica Nanoparticles: Unique Scaling Behavior in the Concentrated Polymer Brush Regime. *Macromolecules* **2017**, *50*, 5565−5573.
(60) Stein, J.; Lewis, L. N.; Gao, Y.; Scott, R. A. In Situ Determination of the Active Catalyst in Hydrosilylation Reactions Using Highly Reactive Pt(0) Catalyst Precursors. *J. Am. Chem. Soc.* **1999**, *121*, 3693−3703.
(61) Jiao, Y.; Akcora, P. Assembly of Polymer-Grafted Magnetic Nanoparticles in Polymer Melts. *Macromolecules* **2012**, *45*, 3463−3470.
(62) Street, D. P.; Mah, A. H.; Ledford, W. K.; Patterson, S.; Bergman, J. A.; Lokitz, B. S.; Pickel, D. L.; Messman, J. M.; Stein, G. E.; Kilbey, S. M., II Tailoring Interfacial Interactions via Polymer-Grafted Nanoparticles Improves Performance of Parts Created by 3D Printing. *ACS Appl. Polym. Mater.* **2020**, *2*, 1312−1324.
(63) Nava, G.; Yang, T.; Vitali, V.; Minzioni, P.; Cristiani, I.; Bragheri, F.; Osellame, R.; Bethge, L.; Klussmann, S.; Paraboschi, E. M.; Asselta, R.; Bellini, T. Newtonian to non-newtonian fluid transition of a model transient network. *Soft Matter* **2018**, *14*, 3288−3295.
(64) McEwan, M.; Green, D. Rheological impacts of particle softness on wetted polymer-grafted silica nanoparticles in polymer melts. *Soft Matter* **2009**, *5*, 1705.
(65) Ndong, R. S.; Russel, W. B. Effects of molecular weight and volume fraction on rheological properties of PDMS-grafted alumina in PDMS melts. *J. Rheol.* **2011**, *55*, 331−351.
(66) Krieger, I. M.; Dougherty, T. J. A Mechanism for Non-Newtonian Flow in Suspensions of Rigid Spheres. *Trans. Soc. Rheol.* **1959**, *3*, 137−152.
(67) Wen, Y. H.; Lu, Y.; Dobosz, K. M.; Archer, L. A. Structure, Ion Transport, and Rheology of Nanoparticle Salts. *Macromolecules* **2014**, *47*, 4479−4492.
(68) Srivastava, S.; Shin, J. H.; Archer, L. A. Structure and rheology of nanoparticle−polymer suspensions. *Soft Matter* **2012**, *8*, 4097.
(69) Minami, S.; Watanabe, T.; Suzuki, D.; Urayama, K. Rheological properties of suspensions of thermo-responsive poly(N-isopropylacrylamide) microgels undergoing volume phase transition. *Polym. J.* **2016**, *48*, 1079−1086.
(70) Cheng, L.; Cao, D. Aggregation of polymer-grafted nanoparticles in good solvents: A hierarchical modeling method. *J. Chem. Phys.* **2011**, *135*, No. 124703.
(71) Kim, S. A.; Archer, L. A. Hierarchical Structure in Semicrystalline Polymers Tethered to Nanospheres. *Macromolecules* **2014**, *47*, 687−694.
(72) Choudhury, S.; Agrawal, A.; Kim, S. A.; Archer, L. A. Self-suspended suspensions of covalently grafted hairy nanoparticles. *Langmuir* **2015**, *31*, 3222−3231.
(73) Tsyba, V. T. Infrared Spectra and the Structure of Poly-1,1-dimethylsilicocyclobutane. *Polym. Sci. U.S.S.R.* **1968**, *10*, 2275−2284.
(74) Kawahara, S.; Nagai, A.; Kazama, T.; Takano, A.; Isono, Y. Preparation of Poly(1,1-dimethyl silabutane) by Anionic Polymerization and Its Crystallization. *Macromolecules* **2004**, *37*, 315−321.
(75) Qiu, W.; Pyda, M.; Nowak-Pyda, E.; Habenschuss, A.; Wunderlich, B. Reversibility between Glass and Melting Transitions of Poly(oxyethylene). *Macromolecules* **2005**, *38*, 8454−8467.
(76) Burgaz, E. Poly(ethylene-oxide)/clay/silica nanocomposites: Morphology and thermomechanical properties. *Polymer* **2011**, *52*, 5118−5126.
(77) Jimenez, A. M.; Krauskopf, A. A.; Pérez-Camargo, R. A.; Zhao, D.; Pribyl, J.; Jestin, J.; Benicewicz, B. C.; Müller, A. J.; Kumar, S. K. Effects of Hairy Nanoparticles on Polymer Crystallization Kinetics. *Macromolecules* **2019**, *52*, 9186−9198.
(78) Kim, S. A.; Archer, L. A. Hierarchical Structure in Semicrystalline Polymers Tethered to Nanospheres. *Macromolecules* **2014**, *47*, 687−694.

https://dx.doi.org/10.1021/acs.chemmater.0c00528
Chem. Mater. 2020, 32, 3990−4001